Room Temperature Persistent Photoconductivity in Barium Calcium Titanate

Syeed E. Ahmed, ^{1,2} Violet M. Poole, ⁴ Jani Jesenovec, ^{1,3} Benjamin L. Dutton, ^{1,3} John S.

McCloy^{1, 3} and Matthew D. McCluskev ^{1, 2, 3, 4, *}

¹ Materials Science and Engineering, Washington State University, Pullman, Washington 99164,

USA

² Department of Physics and Astronomy, Washington State University, Pullman, Washington

99164, USA

³ Institute of Materials Research, Washington State University, Pullman, Washington 99164,

USA

⁴ Klar Scientific, Pullman, Washington 99163, USA

*mattmcc@wsu.edu

ABSTRACT

Barium calcium titanate (Ba_{1-x}Ca_xTiO₃, BCTO) annealed under a flowing humid 2%

hydrogen-argon gas mixture exhibits room-temperature persistent photoconductivity (PPC). The

annealing atmosphere was chosen to produce substitutional hydrogen impurities that can be

photoexcited, leading to the PPC phenomenon. The threshold photon energy for PPC in a BCTO

crystal with x = 0.15 is 2.7 eV, lower than that for BaTiO₃ and SrTiO₃ (2.9 eV). A significant

increase in mid-infrared absorption, attributed to free carriers, was correlated with a drop in

electrical resistance. This effect showed persistence after several days at room temperature.

Annealing the sample in air erased the PPC, indicating that the process is reversible.

ORCiD:

Dutton: 0000-0003-1272-130X

Jesenovec: 0000-0002-5937-6657

McCluskey: 0000-0002-0786-4106

McCloy: 0000-0001-7476-7771

1

INTRODUCTION

Barium titanate, BaTiO₃ (BTO) is a lead-free transparent perovskite material used in electronic devices due to its large dielectric constant, ferroelectricity, and piezoelectric characteristics [1–3]. Among photorefractive perovskite oxides, BTO is a promising candidate owing to its physical properties [4–6], strong holographic sensitivity [7], and large electrooptic coefficients [8]. BTO has a wide range of applications in piezoelectric transducers, actuators, microwave electronics, infrared detectors, multi-layer ceramic capacitors (MLCCs), pulse generators, voltage tuners, and charge storage devices [9–11]. Furthermore, the optical applications of BTO include image processing, optical signal amplification, and optical data storage [12].

BTO is ferroelectric at room temperature with the tetragonal space group *P4mm*. At the growth temperature, hexagonal BTO crystals are generated from a melt of stoichiometric composition [13]. A reconstructive phase transition to the cubic form begins at 1450°C [13], at which point the crystals can be damaged due to cracking. As a result, cubic BTO must be produced at temperatures below 1400°C from solutions with an excess of TiO₂ [14] or from KF fluxes [15], which can lead to inclusions and low growth rates [16–18].

Advancements in high performance microelectronics [19] require MLCCs to increase the operating temperature range to 150°C. Studies found that substituting the Ba site in BTO with metal ions can tailor its working temperature range [20]. Furthermore, alkaline earth metal dopants are recognized for producing a variety of physical features, including ferroelectricity and structural changes, and play a key role in reducing electrical resistance [21,22] in BTO-based semiconductors. Calcium on the barium site can help prevent the formation of the undesirable

hexagonal phase [21] and can lower the orthorhombic to tetragonal phase (T_{O-T}) transition temperature. The substitution of Ca in BTO has a considerable influence on the Curie temperature (T_C) and electrical characteristics [23–25]. In addition, calcium alloying can change the dielectric constant and introduce enhanced piezoelectric properties [26–28].

The local displacement of Ti atoms is known for driving the ferroelectricity and dielectric responses in BTO [29,30]. Perfect BTO crystals have small piezoelectric coefficients and low Curie temperatures ($T_C = 120$ °C) [31]. Doping the pure BTO crystal with calcium to form a barium calcium titanate (Ba_{1-x}Ca_xTiO₃, BCTO) ceramic solid solution has sparked considerable interest due to its wide range of electromechanical properties. [32] The substitution of barium with calcium in BTO enhances the electrical and mechanical responses of the host crystal. It prevents the onset of the unwanted hexagonal phase from forming, allowing the formation of large single crystals. The substitution stabilizes the tetragonal phase, which is the active phase at ambient temperatures [14,33].

Persistent photoconductivity (PPC) is a light-induced photocurrent that lingers after the termination of the excitation source. Room-temperature PPC in strontium titanate (STO) has been demonstrated with sub-bandgap light (~2.9 eV) [34]. BTO showed a similar PPC effect after illumination [35]. Oxygen and hydrogen are the critical components responsible for inducing PPC in STO [36], where a hydrogen atom inside an oxygen vacancy shifts to an interstitial site adjacent to a strontium vacancy, releasing an electron to the conduction band during the process. The same model may also be able to explain the kinetics behind room-temperature PPC in BCTO, the subject of this paper.

EXPERIMENTAL METHODS

BCTO samples were grown using the vertical gradient freeze (VGF) method in an iridium (Ir) crucible (70 mm height, 70 mm diameter) under an inert atmosphere. The precursor powders were BaO (187.05 g), CaO (15.53 g), and TiO₂ (97.43 g). A nominal [Ca]/[Ba] ratio of $x \sim 0.2$ was chosen to minimize the melting point ($\sim 1600^{\circ}$ C). There was little to no evaporation of the BCTO during the growth. Large polycrystal grains of BCTO crystals yielded by the growth were trimmed into $\sim 5 \times 5$ mm² substrates that were 0.5 - 1.0 mm thick. The surfaces were polished on a glass slide with alumina grinding medium down to 0.9 μ m. Sample orientations obtained via the VGF technique were random. As discussed in the Results section, the measured composition was slightly lower than the precursor ratio of 0.2. Powder x-ray diffraction spectra are consistent with the tetragonal perovskite crystal structure (Supplementary Figure S1).

BCTO samples were annealed in a horizontal tube furnace under a flowing gas mixture of humid argon and 98% argon + 2% hydrogen gas. The humid argon was formed by blowing ultrahigh purity argon through high-performance liquid chromatography (HPLC) grade water. The gas sources were combined, and the relative humidity was measured and maintained at \sim 40% throughout the annealing process.

Before switching on the furnace, the annealing chamber was purged for 30 minutes with the gas mixture at a rate of 2.0 standard cubic feet per hour (scf/h). Purging reduces any remaining ambient gases trapped within the sealed chamber. The furnace was then switched on, and the sample was annealed for an hour at 1200°C with a temperature ramp rate of 550°C/h.

The complete gas tube assembly was transported outside the furnace after the hour-long thermal treatment to a point that the region containing the sample could undergo cooling in the dark. The gas continued to flow for another hour, further assisting in sample cooling. The annealing treatment led to a slight darkening of the sample (Supplementary Figure S2), presumably due to free-carrier absorption and/or point defects.

All measurements were taken at room temperature. Raman spectroscopy was performed using a Klar Mini Pro microscope. The microscope was equipped with a fiber-coupled 532 nm CW laser and an Ocean Insight QE Pro spectrometer. The laser excitation power at the sample surface was set to 20 mW with an integration time of 8 s. The excitation laser did not generate any phase changes, despite its comparatively high laser power density [37,38].

A Bomem DA8 Fourier transform infrared (FTIR) spectrometer fitted with a SiC source, an InSb detector, and a KBr beam splitter was used to acquire IR spectra. At room temperature, IR spectra were collected in over a range of 1800 – 6000 cm⁻¹. Light emitting diodes (LEDs) were installed inside the sample chamber to illuminate the BCTO crystals during data acquisition. Spectra were collected in ascending order of photon energy during both the light-off and light-on conditions. The LED intensity was adjusted by keeping the current supply constant at 0.8 A. To compute the change in IR absorbance, the post-LED treated spectra were compared to the original spectrum recorded before any light exposure. Two-point electrical measurements of the BCTO samples were performed using pressed indium contacts and a Fluke digital multimeter. Current-voltage plots showed linear behavior (Supplementary Figure S3).

RESULTS

The chemical composition of the BCTO crystal was investigated using energy dispersive spectroscopy (EDS). The EDS profile in Fig. 1 shows overlapping Ba and Ti peaks within the energy resolution. The presence of O and Ca also be seen in the EDS profile. The EDS spectra were analyzed by the onboard software, and just 2.88 at.% Ca was found. However, this value was influenced by the inaccurate Ba and Ti concentrations. The Ca content is estimated to be ~14.5% by

$$\frac{x}{3} = \frac{[Ca]}{[0]} \tag{1}$$

$$x = \frac{2.88}{59.53} \times 3 \approx 14.5\% \tag{2}$$

where [Ca] and [O] are the measured at.% of Ca and O, respectively. The estimates account for the overlapping Ba and Ti peaks by considering the O at.% as a normalization constant.

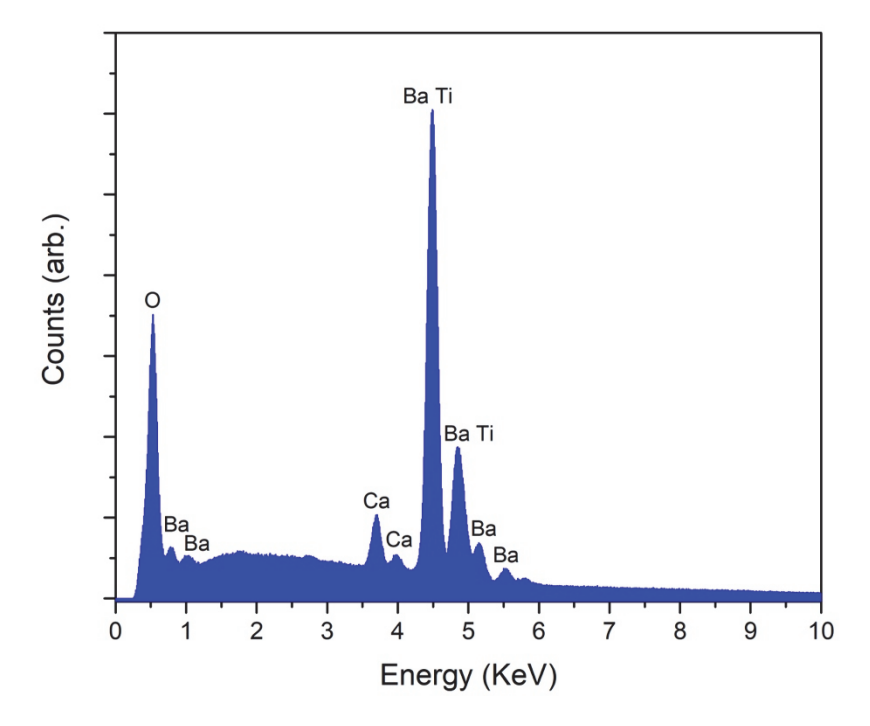


Figure 1: EDS spectrum of a BCTO crystal.

Raman measurements were carried out at room temperature on a commercially available (MTI) one-side polished, $10 \times 10 \times 0.5$ mm, (100) orientated single crystal BTO grown from the top-seeded solution method, as well as the BCTO crystal. The Raman peaks of BTO crystal are located at 172, 275, 515, and 707 cm⁻¹ (Fig. 2) [39]. BCTO has peaks near 150 cm⁻¹ and 250 cm⁻¹, which are ~25 cm⁻¹ lower than the corresponding BTO modes [39]. However, the peak at 515 cm⁻¹ is nearly identical to that in BTO. The 722 cm⁻¹ peak is unique to BCTO in the tetragonal phase [40]. The sharp 123 cm⁻¹ peak is due to the breaking of selection rules caused by Ca disorder in the BCTO lattice [39].

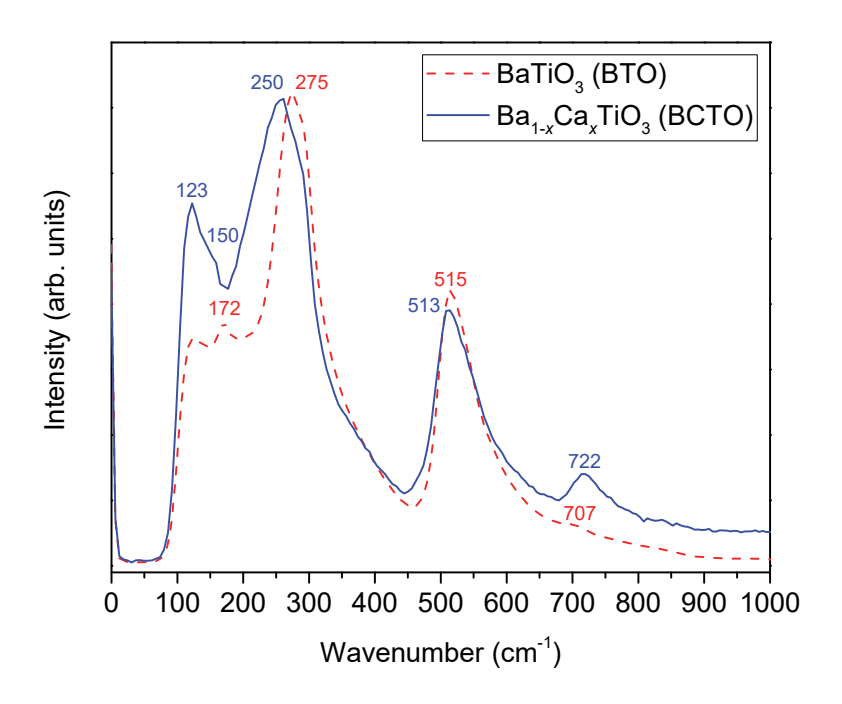


Figure 2: Raman spectra of BTO and BCTO.

A. Photo-induced onset of PPC

Electrical measurements may be used to directly examine the change in conductivity; however, an increase or reduction in the optical absorption in the IR region of the spectrum also correlates to a change in the free-carrier absorption [41]. In BCTO, we studied PPC by analyzing a change in absorbance in the IR spectra; a decrease in transmitted IR intensity links to an increase in free-carrier absorption.

Figure 3 shows the IR transmission intensity of the BCTO sample after LED exposures ranging from 1.98 eV to 3.06 eV. The unexposed crystal is represented by the dotted black spectrum. The IR transmission intensity decreased significantly after the sample was exposed to higher-energy LEDs, with a threshold of 2.72 eV (455 nm).

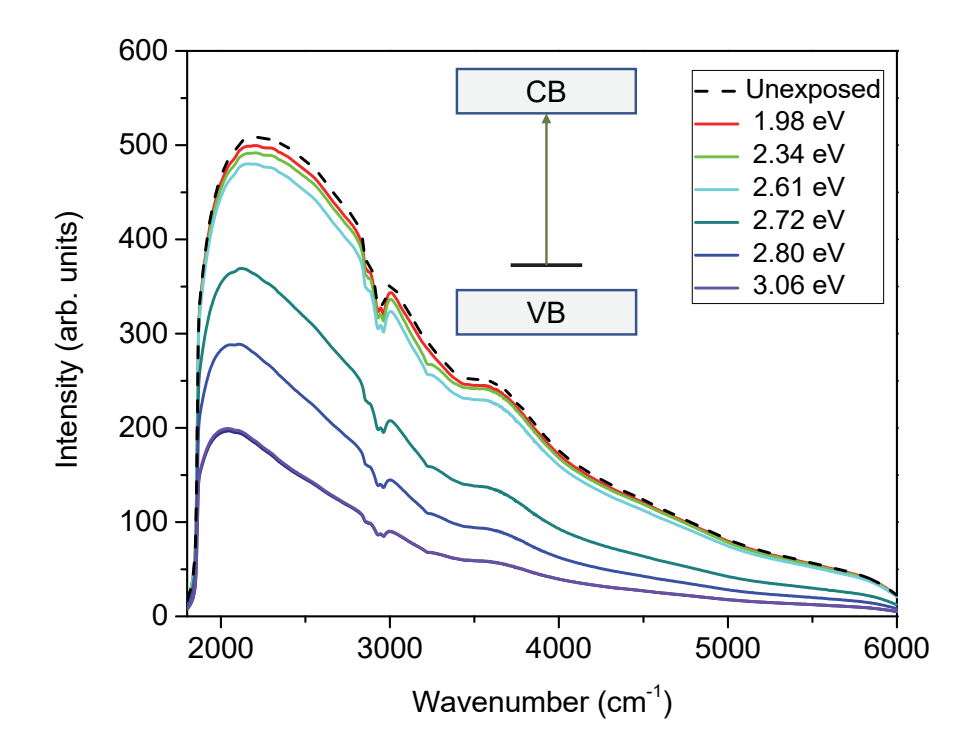


Figure 3: IR transmission spectra of the annealed BCTO crystal after successive exposure to LEDs. The significant reduction in transmission intensity following light exposure with a threshold of 2.72 eV is consistent with PPC. Inset: Conduction band (CB), valence band (VB), and defect level. The 2.72 eV transition from the defect level to the CB is indicated by the vertical arrow.

Figure 4 depicts the change in IR absorbance after LED exposure. To compute the change in absorbance, the post-LED exposed spectra were compared to the pre-exposed spectrum of the sample. Photons with energy below 2.72 eV had no discernible effect. However, illuminating photons with energy starting at 2.72 eV up to 3.06 eV generated a considerable and broad increase in the absorbance spectrum. This effect can be related to an increase in free-carrier density generated by photons with energies ≥ 2.72 eV. The peak around 3220 cm⁻¹ is attributed to an O−H stretching vibration, the origin of which is not known.

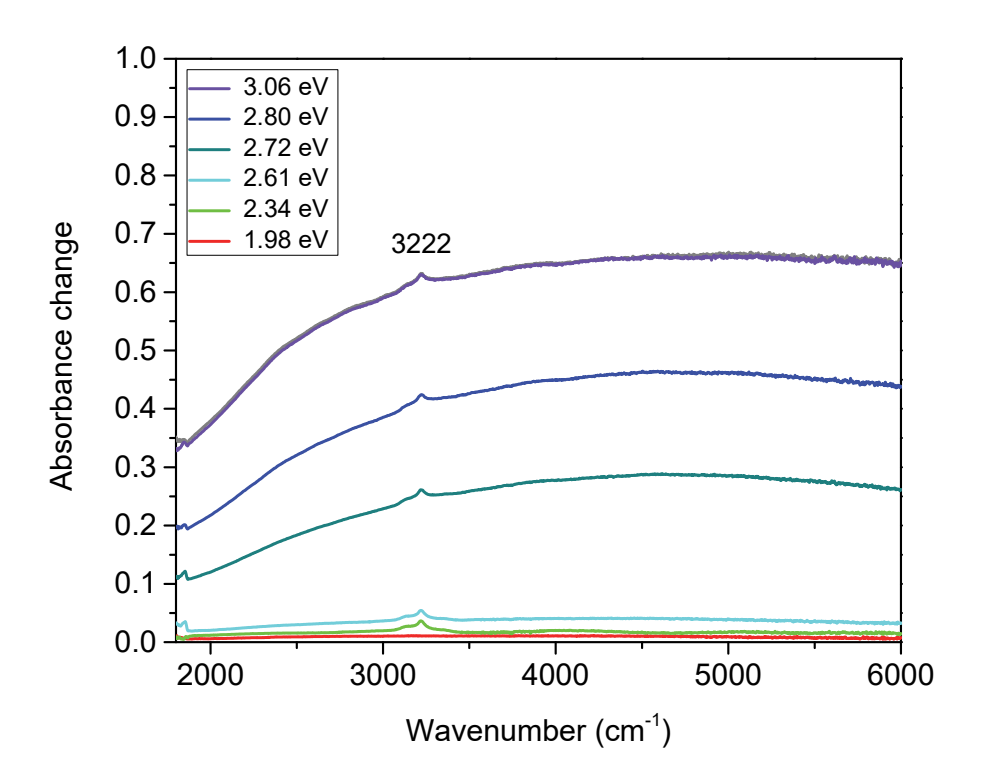


Figure 4: IR absorbance spectra of the annealed BCTO crystal after successive exposure to LEDs. After annealing, the unexposed spectrum (I_0) was used to establish a baseline. Absorbance values are given by $log_{10}(I_0/I)$, where I is the spectrum after exposure.

B. PPC lifetime

The change in IR transmission spectra after 3.06 eV LED exposure is seen in Fig. 5. The spectra were taken in 24-hour increments for a total of 168 hours. The data shows that the transmission intensity begins to increase slowly after LED treatment.

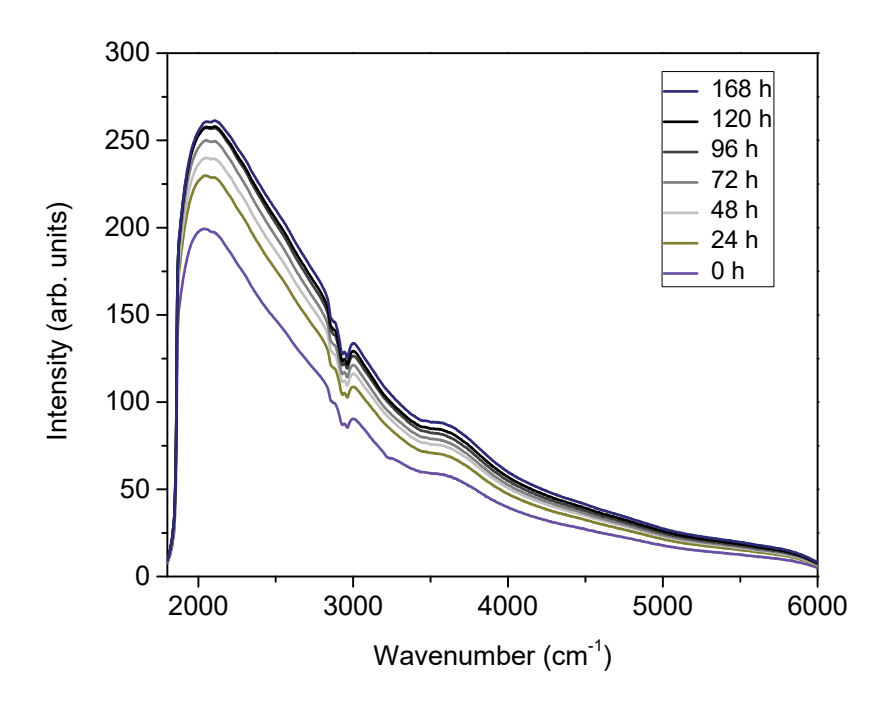


Figure 5: FTIR transmission spectra after 3.06 eV LED exposure.

The IR absorbance change was observed for seven days to assess the duration of PPC effect post 3.06 eV LED illumination (Fig. 6). The sample was shielded from visible and UV radiation throughout this period. The spectra were compared to a baseline unexposed spectrum. The results indicate that the photo-induced change in absorbance is long-lasting. The first 24 hours post LED treatment saw the most significant drop in absorbance. The absorbance change beyond the initial 48 hours was minimal. The peak at 3220 cm⁻¹ was gone 24 hours after illumination.

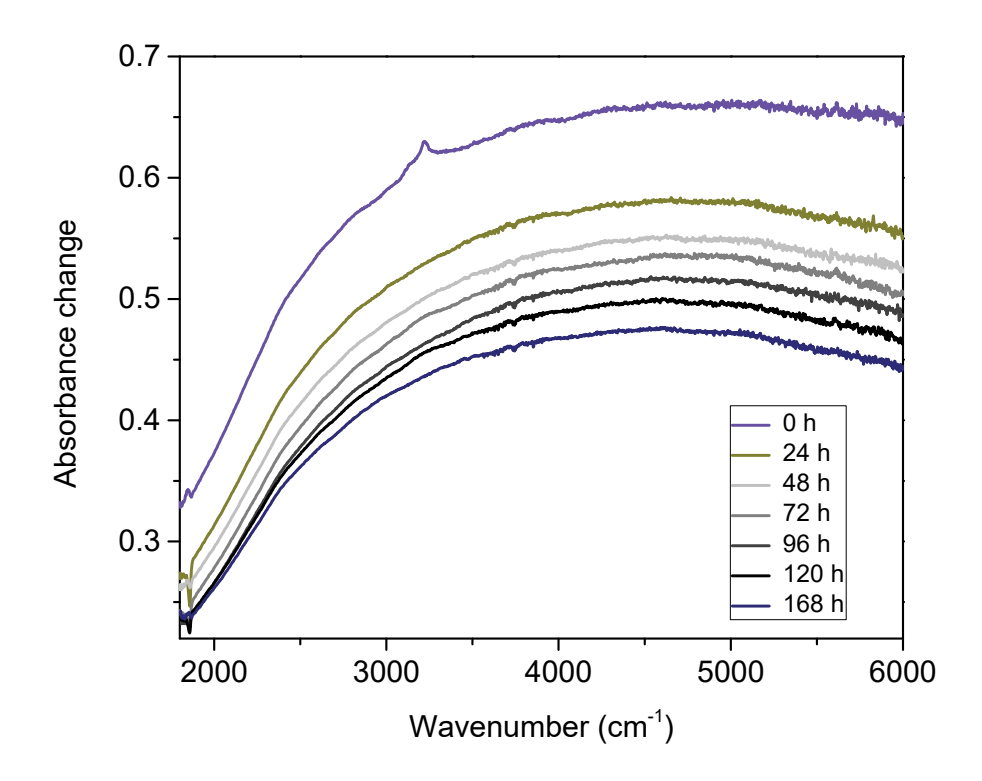


Figure 6: Change in IR absorbance spectra after 3.06 eV LED exposure.

C. PPC reset

The PPC effect can be erased by heating the crystal to 400 °C for 30 minutes in the air. This effectively restores the sample's pre-LED exposure state. Heating the sample on a hot plate, on the other hand, returns the sample's transmission to near-pre-annealing levels, suggesting that the photo-induced PPC effect may be erased. Figure 7 shows that the induced PPC effect resets following the hot plate treatment, indicating that the BCTO crystals can be restored to their initial state for reuse.

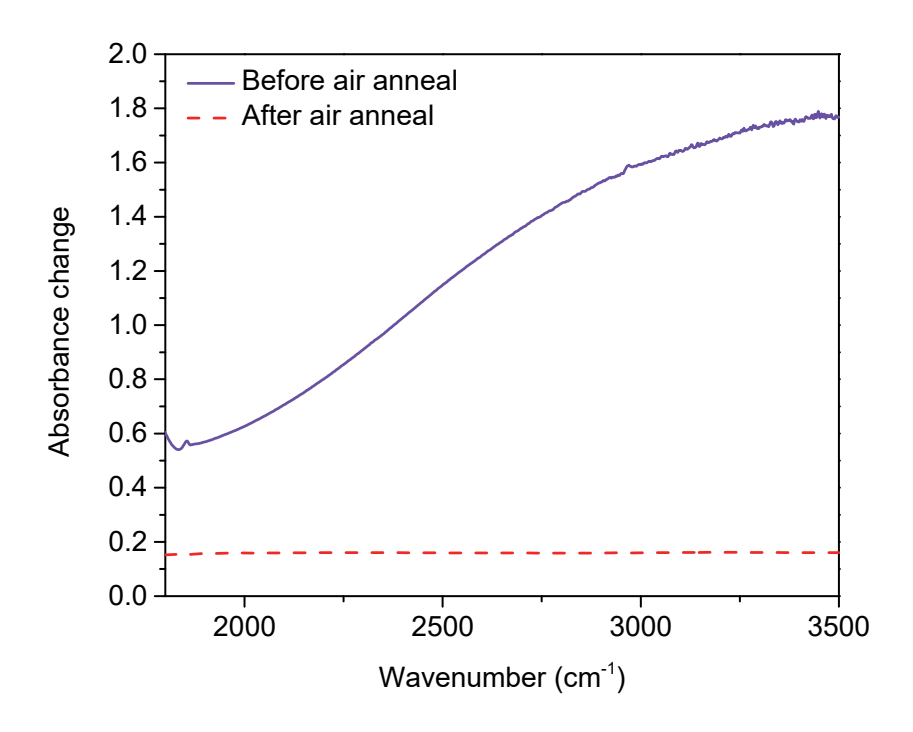


Figure 7: The absorbance spectra changed after a 30-minute hot plate treatment at 400°C, suggesting that the BCTO crystal was reset to its pre-annealing state.

D. Electrical measurements

Parallel to the post-exposure lifetime test, two-point electrical measurements with pressed indium contacts were carried out. Prior to light exposure, the initial resistance was measured to be $\sim \! 14~\mathrm{k}\Omega$. The measured resistance reduced to around 9.9 k Ω after exposure to 3.06 eV light, as seen in Fig. 8. During the next 24 hours, this value increased to $\sim \! 10.2~\mathrm{k}\Omega$ and did not change thereafter for up to 7 days.

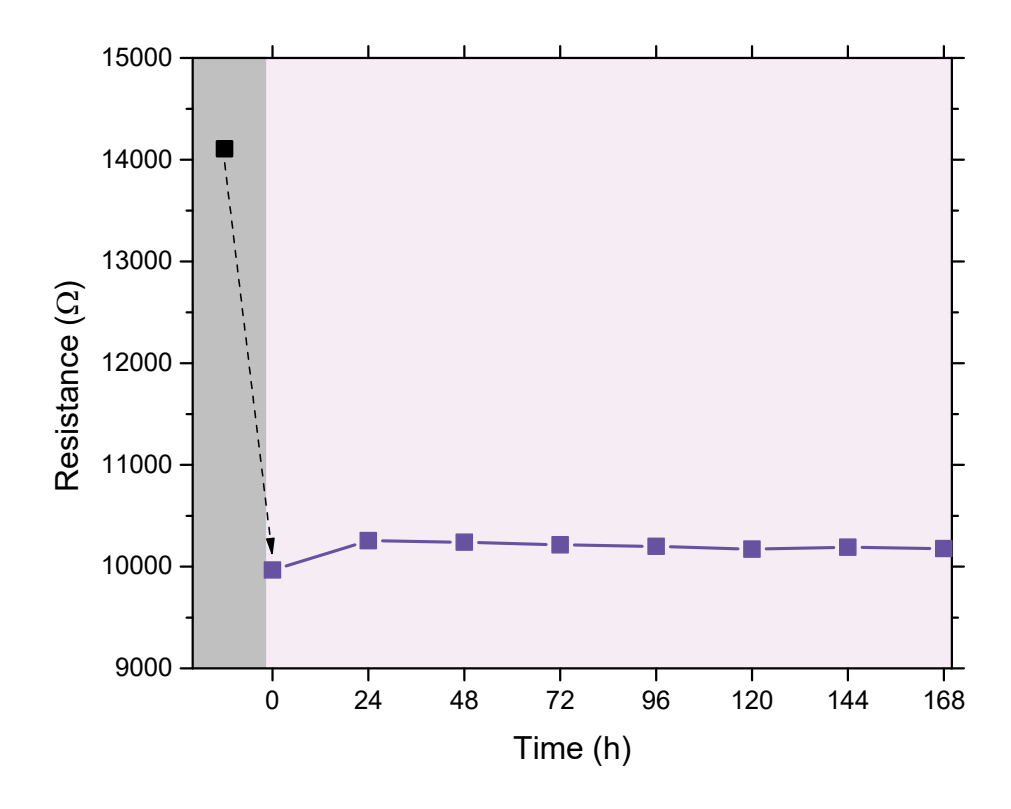


Figure 8: Two-point electrical measurements of annealed BCTO crystal fitted with pressed indium contacts. The grey zone (time < 0) represents resistance before light exposure. The violet zone (time > 0) corresponds to the resistance change after 3.06 eV (405 nm) LED exposure, measured in the dark.

DISCUSSION

The results show that BCTO annealed under flowing hydrogen exhibits room temperature PPC. To explain this effect, we hypothesize that annealing BCTO in a hydrogen-containing environment results in substitutional hydrogen on an oxygen site. [42] Exposure to sub-bandgap light induces substitutional hydrogen to diffuse out and form oxygen vacancies, [42] which act as shallow donors. This leads to excess carriers in the conduction band, resulting in increased conductivity and IR absorption.

The proposed model for PPC in BTO suggests that the hydrogen occupying a V_0 site diffuses in the BTO due to sub-bandgap light exposure and is attracted to an interstitial site near a $(V_{Ba}H)^-$ complex, leading to increased free-carrier concentrations [35]. This O-H bond in this complex is metastable, leading to the persistent photoconductivity. We propose a similar model for PPC in the BCTO crystal. Exposed BCTO annealed in the air at 400°C erased the light-induced PPC effect; in BTO, a similar annealing treatment was not successful in returning the sample to its pre-exposure state.

SUMMARY

In conclusion, when exposed to photons of energy > 2.7 eV, BCTO annealed at 1200 °C in a flowing argon-hydrogen environment shows PPC at ambient temperatures. The optical threshold is slightly lower than that for BTO (2.9 eV) [35] [42]. The observed findings are correlated with the presence of hydrogen in the annealing environment, implying that the PPC mechanism is comparable to that of BTO. [35] Specifically, hydrogen is liberated from the oxygen vacancy site and forms a metastable O-H bond. BCTO can be returned to its preannealed state by annealing it on a hot plate in the air, suggesting that the process is reversible.

Acknowledgments

We thank C. Remple for performing the current-voltage measurement in Supplementary Figure S3. This work was supported by the National Science Foundation under Grant No. DMR-2109334.N

Conflict of Interest Statement

V.M.P. is an employee of Klar Scientific, Inc. and M.D.M. owns equity in the company.

References

- [1] J. F. Ihlefeld, D. T. Harris, R. Keech, J. L. Jones, J.-P. Maria, and S. Trolier-McKinstry, Scaling Effects in Perovskite Ferroelectrics: Fundamental Limits and Process-Structure-Property Relations, Journal of the American Ceramic Society 99, 2537 (2016).
- [2] G. L. Brennecka, J. F. Ihlefeld, J.-P. Maria, B. A. Tuttle, and P. G. Clem, *Processing Technologies for High-Permittivity Thin Films in Capacitor Applications*, Journal of the American Ceramic Society **93**, 3935 (2010).
- [3] Sonia, R. K. Patel, P. Kumar, C. Prakash, and D. K. Agrawal, Low Temperature Synthesis and Dielectric, Ferroelectric and Piezoelectric Study of Microwave Sintered BaTiO3 Ceramics, Ceramics International 38, 1585 (2012).
- [4] R. H. Upadhyay, A. P. Argekar, and R. R. Deshmukh, *Characterization, Dielectric and Electrical Behaviour of BaTiO3 Nanoparticles Prepared via Titanium(IV)*Triethanolaminato Isopropoxide and Hydrated Barium Hydroxide, Bull Mater Sci 37, 481 (2014).
- [5] Y. Wei, Y. Song, X. Deng, B. Han, X. Zhang, Y. Shen, and Y. Lin, *Dielectric and Ferroelectric Properties of BaTiO3 Nanofibers Prepared via Electrospinning*, Journal of Materials Science & Technology **30**, 743 (2014).
- [6] P. Kumar Patel, J. Rani, N. Adhlakha, H. Singh, and K. L. Yadav, *Enhanced Dielectric Properties of Doped Barium Titanate Ceramics*, Journal of Physics and Chemistry of Solids **74**, 545 (2013).
- [7] E. Krätzig, F. Welz, R. Orlowski, V. Doormann, and M. Rosenkranz, *Holographic Storage Properties of BaTiO3*, Solid State Communications **34**, 817 (1980).
- [8] A. R. Johnston, *Dispersion of Electro-Optic Effect in BaTiO3*, Journal of Applied Physics **42**, 3501 (1971).
- [9] V. S. Puli, R. Martinez V, Ashok Kumar, JF Scott, Ram S. Katiyar, Mater. Res. Bull 46, 2527 (2011).
- [10] V. S. Puli, A. Kumar, D. B. Chrisey, M. Tomozawa, J. F. Scott, and R. S. Katiyar, *Barium Zirconate-Titanate/Barium Calcium-Titanate Ceramics via Sol—Gel Process: Novel High-Energy-Density Capacitors*, J. Phys. D: Appl. Phys. **44**, 395403 (2011).
- [11] W. Liu and X. Ren, *Large Piezoelectric Effect in Pb-Free Ceramics*, Phys. Rev. Lett. **103**, 257602 (2009).
- [12] P. Günter and J.-P. Huignard, editors, *Photorefractive Materials and Their Applications 1*, Vol. 113 (Springer-Verlag, New York, 2006).
- [13] D. E. Rase and R. Roy, *Phase Equilibria in the System BaO–TiO2*, Journal of the American Ceramic Society **38**, 102 (1955).
- [14] C. Kuper, R. Pankrath, and H. Hesse, *Growth and Dielectric Properties of Congruently Melting Ba1-XCaxTiO3 Crystals*, Appl Phys A **65**, 301 (1997).
- [15] J. P. Remeika and W. M. Jackson, *A Method for Growing Barium Titanate Single Crystals*, J. Am. Chem. Soc. **76**, 940 (1954).
- [16] P. G. Schunemann, D. A. Temple, R. S. Hathcock, H. L. Tuller, H. P. Jenssen, D. R. Gabbe, and C. Warde, *Role of Iron Centers in the Photorefractive Effect in Barium Titanate*, J. Opt. Soc. Am. B, JOSAB 5, 1685 (1988).
- [17] D. Rytz, B. A. Wechsler, C. C. Nelson, and K. W. Kirby, *Top-Seeded Solution Growth of BaTiO 3, KNbO 3, SrTiO 3, Bi 12TiO 20 and La 2-x, Ba XCuO 4*, Journal of Crystal Growth **99**, 864 (1990).

- [18] S. Ajimura, K. Tomomatsu, O. Nakao, A. Kurosaka, H. Tominaga, and O. Fukuda, *Photorefractive Effect of BaTiO₃ Single Crystals Grown in Inert Atmospheres*, J. Opt. Soc. Am. B, JOSAB **9**, 1609 (1992).
- [19] H. Kishi, Y. Mizuno, and H. Chazono, *Base-Metal Electrode-Multilayer Ceramic Capacitors: Past, Present and Future Perspectives*, Jpn. J. Appl. Phys. **42**, 1 (2003).
- [20] M. T. Buscaglia, V. Buscaglia, M. Viviani, P. Nanni, and M. Hanuskova, *Influence of Foreign Ions on the Crystal Structure of BaTiO3*, Journal of the European Ceramic Society **20**, 1997 (2000).
- [21] Z. Yu, C. Ang, R. Guo, and A. S. Bhalla, *Dielectric Properties of Ba(Ti1-xZrx)O3 Solid Solutions*, Materials Letters **61**, 326 (2007).
- [22] K. Asokan, J. C. Jan, J. W. Chiou, W. F. Pong, P. K. Tseng, I. N. Lin, and IUCr, *X-Ray Absorption Spectroscopy Studies of Ba1-XCaxTiO3*, https://doi.org/10.1107/S0909049501002084.
- [23] L. Zhang, O. P. Thakur, A. Feteira, G. M. Keith, A. G. Mould, D. C. Sinclair, and A. R. West, *Comment on the Use of Calcium as a Dopant in X8R BaTiO3-Based Ceramics*, Appl. Phys. Lett. **90**, 142914 (2007).
- [24] D. F. K. Hennings and H. Schreinemacher, *Ca-Acceptors in Dielectric Ceramics Sintered in Reducive Atmospheres*, Journal of the European Ceramic Society **15**, 795 (1995).
- [25] S. Lee, W. H. Woodford, and C. A. Randall, *Crystal and Defect Chemistry Influences on Band Gap Trends in Alkaline Earth Perovskites*, Appl. Phys. Lett. **92**, 201909 (2008).
- [26] R. C. Pullar, Y. Zhang, L. Chen, S. Yang, J. R. G. Evans, A. N. Salak, D. A. Kiselev, A. L. Kholkin, V. M. Ferreira, and N. McN. Alford, *Dielectric Measurements on a Novel Ba1 XCaxTiO3 (BCT) Bulk Ceramic Combinatorial Library*, J Electroceram **22**, 245 (2009).
- [27] M. R. Panigrahi and S. Panigrahi, *Diffuse Phase Transition and Dielectric Study in Ba0.95Ca0.05TiO3 Ceramic*, Physica B: Condensed Matter **405**, 2556 (2010).
- [28] F. V. Motta, A. P. A. Marques, J. W. M. Espinosa, P. S. Pizani, E. Longo, and J. A. Varela, *Room Temperature Photoluminescence of BCT Prepared by Complex Polymerization Method*, Current Applied Physics **10**, 16 (2010).
- [29] E. A. Stern, *Character of Order-Disorder and Displacive Components in Barium Titanate*, Phys. Rev. Lett. **93**, 037601 (2004).
- [30] R. E. Cohen, Origin of Ferroelectricity in Perovskite Oxides, Nature 358, 6382 (1992).
- [31] T. R. Shrout and S. J. Zhang, *Lead-Free Piezoelectric Ceramics: Alternatives for PZT?*, J Electroceram **19**, 113 (2007).
- [32] X. Chen, L. Wang, Y. Jia, Y. Li, X. Li, W. Dong, B. Wang, and X. Wang, Strongly Enhanced Ferroelectric Performance in Ca-Doped Barium Titanate Coatings Produced by Plasma Electrolytic Oxidation, Ceramics International 45, 13024 (2019).
- [33] H. Veenhuis, T. Börger, K. Peithmann, M. Flaspöhler, K. Buse, R. Pankrath, H. Hesse, and E. Krätzig, *Light-Induced Charge-Transport Properties of Photorefractive Barium-Calcium-Titanate Crystals Doped with Rhodium*, Appl Phys B **70**, 797 (2000).
- [34] M. C. Tarun, F. A. Selim, and M. D. McCluskey, *Persistent Photoconductivity in Strontium Titanate*, Phys. Rev. Lett. **111**, 187403 (2013).
- [35] C. Pansegrau and M. D. McCluskey, *Persistent Photoconductivity in Barium Titanate*, Journal of Applied Physics **131**, 095701 (2022).

- [36] V. M. Poole, J. Huso, and M. D. McCluskey, *The Role of Hydrogen and Oxygen in the Persistent Photoconductivity of Strontium Titanate*, Journal of Applied Physics **123**, 161545 (2018).
- [37] S. E. Ahmed, V. M. Poole, J. Igo, Y. Gu, and M. D. McCluskey, *Localized Phase Transition of TiO2 Thin Films Induced by Sub-Bandgap Laser Irradiation*, Journal of Vacuum Science & Technology A **39**, 053402 (2021).
- [38] S. E. Ahmed, J. Huso, J. R. Ritter, J. Igo, Y. Gu, and M. D. McCluskey, *Insulating Regions in a TiO2 Thin Film Defined by Laser Irradiation*, Journal of Vacuum Science & Technology B **38**, 032203 (2020).
- [39] I. B. Ouni, D. Chapron, H. Aroui, and M. D. Fontana, *Ca Doping in BaTiO3 Crystal: Effect on the Raman Spectra and Vibrational Modes*, Journal of Applied Physics **121**, 114102 (2017).
- [40] Y. Yang, H. Hao, L. Zhang, C. Chen, Z. Luo, Z. Liu, Z. Yao, M. Cao, and H. Liu, *Structure, Electrical and Dielectric Properties of Ca Substituted BaTiO3 Ceramics*, Ceramics International 44, 11109 (2018).
- [41] W. S. Baer, Free-Carrier Absorption in Reduced SrTi\${\mathrm{O}}_{3}\$, Phys. Rev. **144**, 734 (1966).
- [42] Z. Zhang and A. Janotti, Cause of Extremely Long-Lasting Room-Temperature Persistent Photoconductivity in \${\mathrm{SrTiO}}_{3}\$ and Related Materials, Phys. Rev. Lett. 125, 126404 (2020).